

# Proposal for demonstration of long-range cluster state entanglement in the presence of photon loss

Cite as: APL Photonics 2, 066103 (2017); <https://doi.org/10.1063/1.4983822>

Submitted: 07 February 2017 . Accepted: 07 May 2017 . Published Online: 23 May 2017

Thomas Nutz , Antony Milne, Pete Shadbolt, and Terry Rudolph



View Online



Export Citation



CrossMark

## ARTICLES YOU MAY BE INTERESTED IN

[Why I am optimistic about the silicon-photonic route to quantum computing](#)

APL Photonics 2, 030901 (2017); <https://doi.org/10.1063/1.4976737>

[Invited Article: Generation of one-million-mode continuous-variable cluster state by unlimited time-domain multiplexing](#)

APL Photonics 1, 060801 (2016); <https://doi.org/10.1063/1.4962732>

[Invited Review Article: Single-photon sources and detectors](#)

Review of Scientific Instruments 82, 071101 (2011); <https://doi.org/10.1063/1.3610677>

additive manufacturing epitaxial crystal growth cerium oxide polishing powder silver nanoparticles sputtering targets III-IV semiconductors CVD precursors europium phosphors

**AMERICAN ELEMENTS**  
THE ADVANCED MATERIALS MANUFACTURER®

deposition slugs OLED Lighting spintronics solar energy osmium nanoribbons thin films chalcogenides AuNPs GDC Li-ion battery electrolytes 99.999% ruthenium spheres

endoheedral fullerenes copper nanoparticles diamond micropowder CIGS MBE grade materials palladium catalysts flexible electronics beta-barium borate borosilicate glass dysprosium pellets YBCO pyrolytic graphite 3d graphene foam indium tin oxide mesoporous silica raman substrates sapphire windows tungsten carbide InGaAs barium fluoride carbon nanotubes lithium niobate scandium powder

gallium lump glassy carbon nanodispersions InAs wafers laser crystals ultra high purity materials MOFs rare earth metals photovoltaics refractory metals MOCVD organometallics quantum dot superconductors transparent ceramics ultra high purity silicon

*American Elements opens up a world of possibilities so you can **Now Invent!***

Over 15,000 certified high purity laboratory chemicals, metals, & advanced materials and a state-of-the-art Research Center. Printable GHS-compliant Safety Data Sheets. Thousands of new products. And much more. All on a secure multi-language "Mobile Responsive" platform.

perovskite crystals yttrium iron garnet alternative energy h-BN gold nanocubes graphene oxide macromolecules photonics rhodium sponge fiber optics beamsplitters infrared dyes zeolites fused quartz metallocenes platinum ink buckyballs Ti-6Al-4V

**Now Invent.™**  
The Next Generation of Material Science Catalogs

[www.americanelements.com](http://www.americanelements.com)

# Proposal for demonstration of long-range cluster state entanglement in the presence of photon loss

Thomas Nutz,<sup>1,a</sup> Antony Milne,<sup>1,2</sup> Pete Shadbolt,<sup>1</sup> and Terry Rudolph<sup>1</sup>

<sup>1</sup>*Controlled Quantum Dynamics Theory Group, Imperial College London, London SW7 2AZ, United Kingdom*

<sup>2</sup>*Department of Computing, Goldsmiths, University of London, New Cross, London SE14 6NW, United Kingdom*

(Received 7 February 2017; accepted 7 May 2017; published online 23 May 2017)

Photonic cluster states are a crucial resource for optical quantum computing. Recently a quantum dot single photon source has been demonstrated to produce strings of single photons in a small linear cluster state. Sources of this kind could produce much larger cluster states, but high photon loss rates make it impossible to characterize the entanglement generated by quantum state tomography. We present a benchmarking method for such sources that can be used to demonstrate useful long-range entanglement with currently available collection/detection efficiencies below 1%. The measurement of the polarization state of single photons in different bases can provide an estimate for the three-qubit correlation function  $\langle ZXZ \rangle$ . This value constrains correlations spanning more than three qubits, which in turn provide a lower bound for the localizable entanglement between any two qubits in the large state produced by the source. Finite localizable entanglement can be established by demonstrating  $\langle ZXZ \rangle > \frac{2}{3}$ . This result enables photonic experiments demonstrating computationally useful entanglement with currently available technology. © 2017 Author(s). All article content, except where otherwise noted, is licensed under a Creative Commons Attribution (CC BY) license (<http://creativecommons.org/licenses/by/4.0/>). [<http://dx.doi.org/10.1063/1.4983822>]

## I. INTRODUCTION

Measurement-based quantum computation (MBQC)<sup>1</sup> has become a promising candidate for the most resource-efficient way to build a universal quantum computer. The greatest challenge of MBQC is the generation of a sufficiently large entangled resource state. This step is critical because only certain types of multi-qubit entanglements are known to enable universal quantum computation,<sup>2</sup> most prominently cluster state entanglement.<sup>3,4</sup>

Photonic systems have been proposed to generate cluster states.<sup>5,6</sup> Recently a complete architecture for a linear optical quantum computer has been developed that relies on the probabilistic fusion of many small entangled states into one large cluster state.<sup>7</sup> In this proposal, the generation of the entangled resource state requires only the generation of many maximally entangled three-photon states, at the cost of a significant overhead of single-photon detection measurements and classical information processing. This overhead could be dramatically reduced by developing deterministic “machine gun” sources of photonic cluster states.<sup>8,9</sup>

In a recent experimental breakthrough,<sup>10</sup> a quantum dot (QD) single photon source has been demonstrated to generate three-qubit cluster states. The time required to characterize the performance of this device using tomography was considerable. A simple estimate shows that although the source is in principle capable of emitting long strings of entangled photons, tomography on larger states is essentially infeasible given the low collection efficiency. Our result makes it possible to characterize the computationally useful entanglement in such long strings of single photons even in the presence

---

<sup>a</sup>nutzat@gmail.com

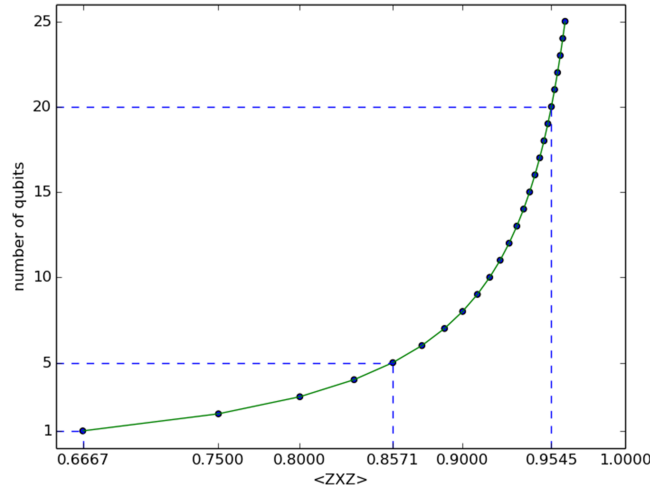


FIG. 1. A sufficiently high value of  $\langle ZXZ \rangle$  guarantees non-zero LE across many qubits. For instance, a value of  $\langle ZXZ \rangle = 0.8571$  (0.9545) is sufficient to demonstrate non-zero LE across 5 (20) qubits. The curve shown is obtained by setting Eq. (1) to zero and plotting  $k - 1$  (number of measured qubits) vs.  $\langle ZXZ \rangle$ .

of photon loss rates as high as reported in Ref. 10. The type of entanglement that makes cluster states a resource for MBQC can be quantified in terms of the localizable entanglement (LE) or the teleportation fidelity as introduced in Section III. We find that given a measured three-photon correlation  $\langle ZXZ \rangle$ , the LE across  $k$  qubits in a state  $\rho$  of at least  $k + 1$  single photons is lower bounded as

$$\text{LE}^{j+k}(\rho) \geq 1 - (k + 1)(1 - \langle ZXZ \rangle), \quad (1)$$

and the teleportation fidelity across  $k$  qubits as

$$F_T(\rho) \geq 1 - \frac{k + 1}{3}(1 - \langle ZXZ \rangle). \quad (2)$$

The three-photon correlation  $\langle ZXZ \rangle$  can be measured using a simple optical setup and in highly lossy systems, as demonstrated in Ref. 10 with the result  $\langle ZXZ \rangle = 0.619 \pm 0.061$ . This measured correlation is close to the value of  $\langle ZXZ \rangle = 2/3$  at which the above bounds become meaningful. As  $\langle ZXZ \rangle \rightarrow 1$ ,  $\text{LE}^{j+k}(\rho) \rightarrow 1$  for any  $k$  as shown in Fig. 1. Hence cluster state entanglement across many qubits can be demonstrated by measuring  $\langle ZXZ \rangle$  in future experiments.

## II. EXPERIMENTAL PROTOCOL TO GENERATE AND VERIFY PHOTONIC CLUSTER STATES

A protocol for the experimental realization of photonic cluster states has been proposed in Ref. 8. We review this proposal and the measurement setup proposed in Ref. 11 with focus on practical implementation.

Certain single photon sources, such as charged QDs or  $\text{NV}^-$  centres in diamond,<sup>12</sup> can be used to produce entanglement between an emitter spin and the polarization of single photons. In these sources the two ground states of a trapped spin couple via degenerate optical transitions to two excited states, whereby the transitions obey strict selection rules. An example of such a system is given by self-assembled indium-arsenide QDs, where the spin up/down state couples via right/left handed circularly polarized light to the respective spin up/down charged exciton states.<sup>13</sup> Pulsed excitation and subsequent decay via single photon emission lead to a string of time-binned photons. The quantum state of these single photons and the emitter spin is the linear cluster state if the emitter spin is coherently rotated by  $90^\circ$  in the Bloch sphere in between excitation pulses.<sup>8</sup>

Given that a single photon source capable of repeated emission has been set up, an experiment needs to verify that the photons emitted are in the linear cluster state or close enough for a given quantum information processing task of interest. An optical setup has been proposed<sup>11</sup> for the

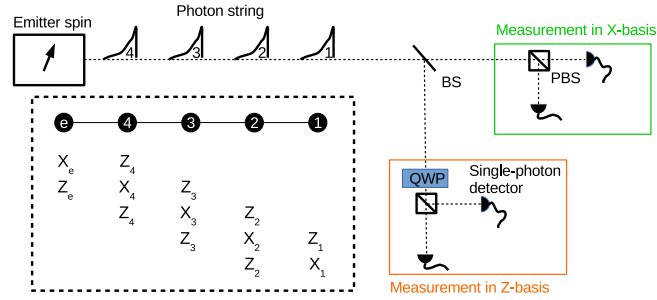


FIG. 2. Cluster state source experiment with the measurement setup. A trapped emitter spin is repeatedly excited, each time emitting a photon into a spatial mode represented by the thin dashed line. The sketch shows a snapshot at a time after the emission of the fourth photon. Abbreviations: BS—beam splitter; PBS—polarizing beam splitter; QWP—quarter waveplate. The inset in the dashed box shows the graph state representation of the state, where each labelled circle represents a qubit and the lines in between represent the cluster state entanglement. Below are the stabilizer generators of the state, where  $X_e Z_4$  is short for  $X_e \otimes Z_4$ .

characterization of photonic cluster state sources, and a simplified version is shown in Fig. 2. The data obtained with this setup consist of time-tagged single-photon detection events (“clicks”). A click in one of the four detectors corresponds to a projective single-qubit measurement in either the  $X$  or  $Z$  Pauli basis. For example, if the upper right detector in Fig. 2 clicks during the second timebin, we may interpret this event as the projection of qubit 2 onto the  $+1$  eigenstate of the Pauli operator  $X$ .

The data collected consist of a large number of time-tagged measurement outcomes of the form “qubit 1 measured  $+1$  in  $X$ , qubit 2 got lost, qubit 3 measured  $-1$  in  $Z$ , . . . .” Averages of these measurement outcomes yield expectation values of Pauli operators. For instance, the expectation value  $\langle Z_3 \otimes X_4 \otimes Z_5 \rangle$  (subscripts label the timebins) can be obtained in the following way:

1. collect sufficiently many outcomes of the event sequence “photon 3 measured in the  $Z$  basis, photon 4 in  $X$ , photon 5 in  $Z$ ;”
2. multiply the outcomes of each such triplet of measurement outcomes;
3. the average of these products is an estimate of the expectation value  $\langle Z_3 \otimes X_4 \otimes Z_5 \rangle$ .

We call the number of single-qubit Pauli operators in a multi-qubit Pauli operator the support of this operator. The operator  $Z_3 \otimes X_4 \otimes Z_5$ , for example, has support on three qubits. Clearly the probability of detecting a sequence of photons at the relevant detectors for a given operator decays exponentially with the support of the operator and the inverse of the photon detection probability in the presence of photon loss.

Repeatedly generating the state of  $n$  photons and collecting all  $4^n - 1$  Pauli expectation values constitute full quantum state tomography and yields all information obtainable on the state of these  $n$  qubits. This method, however, is clearly not scalable, and we need to come up with a more efficient way to characterize the cluster state source. Given photon loss, it is in particular the support of the expectation values needed that we wish to minimize.

To understand the role of photon loss and the measurements feasible with today’s technology, we consider the experiment presented in Ref. 10. The overall efficiency was such that roughly one photon per 700 timebins was detected. Using a setup as in Fig. 2, the probability of getting three consecutive photons on the  $Z$ ,  $X$ , and  $Z$  detectors, respectively, is given by  $p_s = (\frac{1}{2} \frac{1}{700})^3$ . At the excitation rate of 76 MHz reported in Ref. 10, this probability translates to about 30 min of integration time for a single event contributing to the estimate of some  $\langle Z_{i-1} X_i Z_{i+1} \rangle$ . Measuring a three-qubit expectation value is therefore already feasible and has in fact been demonstrated.<sup>10</sup> Expectation values of larger support, however, require higher efficiency.

### III. VERIFYING CLUSTER STATE ENTANGLEMENT IN LARGE PHOTONIC STATES USING THE $\langle ZXZ \rangle$ BOUND

There is a variety of experiments on sources of entangled photons which could potentially produce cluster states. For such a source to enable MBQC, all (or at least a certain fraction considering a loss

tolerant encoding) of the single photons of a large state need to be detectable. Furthermore, this large state needs to have a certain type of entanglement that enables MBQC. In this work, we focus on the second requirement: Assume that a source produces a large photonic state, but the photon collection efficiency is low. Can one at least make sure that the entanglement present in this large state is such that the state would be sufficient for MBQC if photon collection efficiency was improved?

Our result enables this demonstration of useful entanglement in large photonic states with high losses. Before we present our result, we need to introduce two measures of cluster state long-range entanglement, since distance measures such as fidelity to an ideal cluster state do not capture the computational power of an experimentally produced mixed state.

The *localizable entanglement* (LE) can be taken as such a figure of merit. To understand why this quantity is suited for cluster state experiments, let us consider the ideal linear cluster state on  $n$  qubits. A sequence of single-qubit measurements in the  $X$  or  $Y$  basis on qubits 2 to  $n - 1$  results in a maximally entangled state of the unmeasured qubits 1 and  $n$  (see Fig. 3 for an example). If the  $n$  qubit state prior to the measurements was a faulty cluster state, then the two-qubit state resulting from the measurement sequence is generally not maximally entangled, and this resulting two-qubit entanglement might depend on the choice of measurement bases as well as the outcomes of these measurements.

The localizable entanglement  $LE^{ij}(\rho)$  is defined with respect to two qubits  $i, j$  in a state  $\rho$  of  $n$  qubits as the maximum average entanglement between  $i$  and  $j$  that can be obtained by means of a sequence of single-qubit measurements on the other  $n - 2$  qubits in  $\rho$ .<sup>14</sup> The maximum is taken over all measurement bases, while the average refers to all possible measurement outcomes, and we take concurrence to be the two-qubit entanglement measure. The task of benchmarking a cluster state source is accomplished by lower bounding the localizable entanglement of the state that it produces.

A second measure of cluster state entanglement is the teleportation fidelity. Now assume that one wishes to perform a joint measurement on qubit 1 of a linear state such as the one shown in Fig. 3 and some single-qubit state  $|\psi\rangle$  to be teleported, followed by a sequence of single-qubit measurements on qubits 2 to  $n - 1$ . Using a perfect linear cluster state, it is possible to retrieve the state  $|\psi\rangle$  on qubit  $n$ , but any errors on the linear cluster state will bring down the fidelity of this operation. We take the teleportation fidelity that can be achieved using a faulty  $n$  qubit cluster state  $\rho$  as a second figure of merit for a cluster state source producing  $\rho$ .

We now present our main result. Given that the expectation values  $\langle Z_{i-1}X_iZ_{i+1} \rangle$  on any three neighboring qubits in a linear state  $\rho$  of at least  $k + 1$  qubits are no smaller than some value  $\langle ZXZ \rangle$ , the localizable entanglement is lower bounded,

$$LE^{j+k}(\rho) \geq 1 - (k + 1)(1 - \langle ZXZ \rangle). \quad (3)$$

Furthermore we find that a linear state  $\rho$  with expectation values  $\langle Z_{i-1}X_iZ_{i+1} \rangle \geq \langle ZXZ \rangle$  enables a quantum teleportation channel across  $k$  qubits of fidelity

$$F_T \geq 1 - \frac{k + 1}{3}(1 - \langle ZXZ \rangle). \quad (4)$$

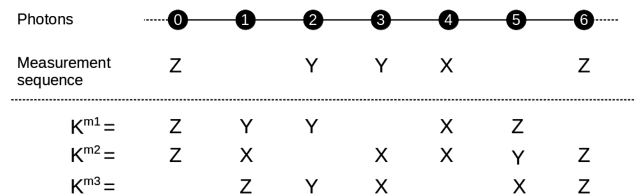


FIG. 3. Example of a stabilizer triplet corresponding to an entanglement localizing measurement sequence. The dashed lines to the left and right of photons 0 and 6 indicate that we are looking at a segment of a long linear cluster state. The Z measurement cut out a linear cluster state on qubits 1 to 5. The X and Y measurements (like any measurements in a basis in the equatorial plane of the Bloch sphere) lead to a maximally entangled two-qubit state of qubits 1 and 5. Denoting stabilizer generators as  $K_i = Z_{i-1}X_iZ_{i+1}$ , one finds that the stabilizers  $K^{m_i}$  that commute with the measurement sequence are  $K^{m_1} = K_1K_2K_4$ ,  $K^{m_2} = K_1K_3K_4K_5$ , and  $K^{m_3} = K_2K_3K_4$ . Hence we have  $m_1 = 3$ ,  $m_2 = 4$ , and  $m_3 = 3$ . See Ref. 15 for background on the stabilizer formalism.

This result makes it possible to demonstrate useful long-range entanglement in large photonic states with low photon collection efficiency. Given that  $\langle ZXZ \rangle > 2/3$ , the LE of the state produced is guaranteed to be nonzero and the teleportation fidelity must be higher than that provided by any separable state. As  $\langle ZXZ \rangle$  approaches unity, the LE tends to the maximum value found in ideal cluster states as shown in Fig. 1. Experimental control parameters can therefore be optimized by looking for a maximum in  $\langle ZXZ \rangle$ . We refer to Eq. (3) as the  $\langle ZXZ \rangle$  bound and to Eq. (4) as the fidelity bound in the following.

#### IV. PROOF AND PROPERTIES OF THE $\langle ZXZ \rangle$ BOUND

##### A. Proof of the $\langle ZXZ \rangle$ bound

The proof of the  $\langle ZXZ \rangle$  bound makes use of the stabilizer formalism.<sup>15</sup> The linear cluster state on  $n$  qubits is the unique eigenstate of the operators  $X_1Z_2$ ,  $Z_{i-1}X_iZ_{i+1} \forall 2 \leq i \leq n-1$ , and  $Z_{n-1}X_n$  with eigenvalues +1 (see Fig. 3 for an example). These operators are called the stabilizer generators of the cluster state. Clearly the cluster state also is the +1 eigenstate of any product of stabilizer generators, called the stabilizers of the cluster state. We denote a stabilizer which is the product of  $m$  stabilizer generators as  $K^m$ .

If all stabilizer generators in some state  $\rho$  of  $n$  qubits have expectation values no smaller than some value  $\langle ZXZ \rangle$ , the expectation values of any stabilizer are lower bounded by

$$\langle K^m \rangle \geq m(\langle ZXZ \rangle - 1) + 1. \quad (5)$$

This bound derives from the following bound on the expectation value of the product of two commuting operators  $P_1$  and  $P_2$ :

$$\langle P_1 P_2 \rangle \geq \langle P_1 \rangle + \langle P_2 \rangle - 1, \quad (6)$$

which follows from

$$\begin{aligned} & \text{Tr}[\frac{1}{2}(\mathbb{1} - P_1)\frac{1}{2}(\mathbb{1} - P_2) \rho] \\ &= \text{Tr}[\frac{1}{4}(\mathbb{1} - P_1 - P_2 + P_1 P_2) \rho]. \end{aligned} \quad (7)$$

$$\geq 0.$$

The latter is true as  $\frac{1}{2}(\mathbb{1} - P_{1,2})$  are projectors and therefore non-negative.

As shown in Appendix A, certain triplets of stabilizer expectation values  $\langle K^{m_i} \rangle$ ,  $i = 1, 2, 3$ , can lower bound the LE of a quantum state  $\rho$ . The value of this lower bound is the entanglement of the two-qubit state  $\rho_B$  defined in Eq. (A1) with  $B_i = K^{m_i}$ . The concurrence of this state is given by<sup>16</sup>

$$C(\rho_B) = \max\{0, \frac{1}{2}(\langle K^{m_1} \rangle + \langle K^{m_2} \rangle + \langle K^{m_3} \rangle - 1)\}. \quad (8)$$

Substituting for  $\langle K^{m_i} \rangle$  from Eq. (5), we obtain

$$C(\rho_B) \geq \frac{1}{2}(m_1 + m_2 + m_3)(\langle ZXZ \rangle - 1) + 1. \quad (9)$$

The operators  $K^{m_i}$  can be found by choosing a sequence of either  $Y$  or  $X$  measurements on qubits 2 to  $n-1$  and updating the set of stabilizer generators of the ideal cluster state so as to account for the state resulting from these measurements. The resulting set of stabilizers contains the three elements  $K^{m_i}$ . An example is presented in Fig. 3. Each  $X$  or  $Y$  measurement appends a stabilizer generator to two of the three operators  $K^{m_i}$  such that

$$m_1 + m_2 + m_3 = 4 + 2(n-2). \quad (10)$$

Substituting this expression into Eq. (9), we arrive at

$$\text{LE}^{1,n}(\rho) \geq 1 - n(1 - \langle ZXZ \rangle). \quad (11)$$

The expression given in Eq. (1) in terms of two qubits labelled  $j$  and  $j+k$  follows by considering the segment of  $k+1$  qubits of a linear state that results from measuring qubits  $j-1$  and  $j+k+1$  in the  $Z$  basis.

The triplet sum  $T = \langle K^{m_1} \rangle + \langle K^{m_2} \rangle + \langle K^{m_3} \rangle$  furthermore lower bounds the fully entangled fraction as introduced in Ref. 17, which in turn gives the fidelity of a teleportation protocol<sup>18</sup> using the linear state  $\rho$  as described above. Hence

$$F_T(\rho) \geq 1 - \frac{n}{3}(1 - \langle ZXZ \rangle). \quad (12)$$

## B. The WC state

The teleportation fidelity bound and the lower bounds to stabilizer expectation values (Eq. (5)) are tight bounds. The  $\langle ZXZ \rangle$  bound has been found to be tight for all examples investigated (see Appendix B). The state that saturates these bounds is the worst-case scenario for the state produced by a cluster state source given knowledge of only  $\langle ZXZ \rangle$ . We call this state the WC state on  $n$  qubits  $\rho_n^{WC}$  and write it as

$$\rho_n^{WC} = \lambda |C_n\rangle\langle C_n| + \frac{1-\lambda}{n} \sum_{i=1}^n Z_i |C_n\rangle\langle C_n| Z_i, \quad (13)$$

where  $|C_n\rangle$  is the linear cluster state on  $n$  qubits. The parameter  $\lambda$  is chosen such that  $\text{Tr}[Z_{i-1} X_i Z_{i+1} \rho_n^{WC}] = \langle ZXZ \rangle$ , i.e.,

$$\lambda = 1 - n \frac{1 - \langle ZXZ \rangle}{2}. \quad (14)$$

The defining property of the WC state is that it saturates all inequalities given in Eq. (5),

$$\begin{aligned} \text{Tr}[K^m \rho_n^{WC}] &= \lambda + \frac{1-\lambda}{n} \sum_{i=1}^n \text{Tr}[K^m Z_i |C_n\rangle\langle C_n| Z_i] \\ &= \lambda + \frac{1-\lambda}{n} (n - 2m) \\ &= m(\langle ZXZ \rangle - 1) + 1. \end{aligned} \quad (15)$$

The second line is obtained by noting that  $K^m$  anticommutes with  $m$  of the  $Z_i$  operators, yielding  $-1$  for  $m$  terms in the sum on the rhs of the first line. The third line follows by substituting  $\lambda$  from (14).

The state  $\rho_n^{WC}$  therefore has a triplet sum  $T$  no higher than the lower bound given by Eq. (5), which means that it saturates the teleportation fidelity bound. Hence Eq. (5) and the teleportation fidelity bound are tight, while the  $\langle ZXZ \rangle$  bound is conjectured to be tight as described in Appendix B.

## V. COMPARISON TO OTHER CHARACTERIZATION METHODS

### A. Process tomography

The experiment reported in Ref. 10 is claimed to demonstrate LE across five photons, although the states produced contained three photons at most. This claim is justified by the complete characterization of the quantum process that entangles the emitter spin with a single photon, then calculating the multi-photon state that would be obtained if this process acted many times, and finally computing the LE of this large state. In this way, LE across arbitrarily many qubits can be demonstrated while never actually producing states containing more than three photons. Moreover this method yields an estimate of the LE actually present in the state generated, rather than lower bounding it.

However the process tomography method relies on the assumption that the spin-photon entangling process is the same over many excitation pulses. The bounds presented here, in contrast, do not make any assumption on the physical mechanism that generated the photon string. If the cluster state source is to be used in any MBQC protocol, then it must actually generate large entangled photonic states. In that case, the supposed state extrapolated from the process tomography can be checked against the measurements on the state generated in the experiment via the  $\langle ZXZ \rangle$  bound.

An advantage of lower bounding LE using  $\langle ZXZ \rangle$  rather than computing it from a process map is the scalability. The process tomography method applied to an  $n$  photon state involves the computation of a  $2^n \times 2^n$  density matrix and estimation of the LE from these data (the LE of a quantum state is generally not exactly computable). The  $\langle ZXZ \rangle$  bound seems therefore better suited for the optimization of experimental parameters during the realization of the experiment and demonstration of LE across many qubits than the computationally intense process tomography approach.

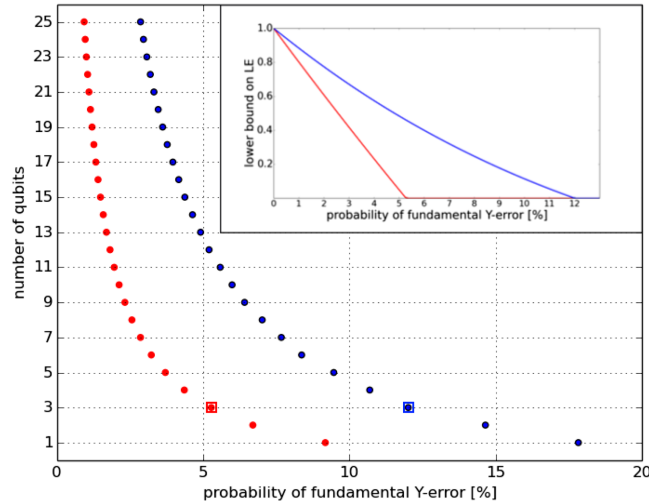


FIG. 4. The  $\langle ZXZ \rangle$  bound is generally lower than the direct bound. In the main plot, the maximum number of qubits across which the direct bound (blue) and the  $\langle ZXZ \rangle$  bound (red) guarantee non-zero LE is shown. The x-axis gives the probability of a Pauli  $Y$ -error on the emitter spin (fundamental error) before each single-photon emission. The inset shows the value of LE that each bound establishes across three qubits, again plotted against the probability of a fundamental  $Y$ -error. The highlighted data points in the main plot correspond to the points in the inset plot where each curve hits zero.

## B. The direct bound

The three expectation values  $K^{m_i}$  can in principle be measured directly using a setup as in Fig. 2 with another arm to measure in the  $Y$  basis. Clearly this information will lower bound the LE, and we call this bound presented in Ref. 11 the direct bound. The direct bound will in general be higher than the  $\langle ZXZ \rangle$  bound, except for the unrealistic scenario where the source produces a WC state. The downside is, however, that the support of the operators  $K^{m_i}$  that need to be measured in order to demonstrate LE across  $n$  qubits grows linearly with  $n$ , which makes it exponentially hard to measure the direct bound. Hence the direct bound is not useful yet for demonstrating long-range entanglement given the low photon collection efficiency of current experiments. Given higher efficiency, there is a trade-off between saving measurement resources and demonstrating a high value of LE.

An interesting scenario to investigate this trade-off is a cluster state source as proposed in Ref. 8 subject to uncorrelated Pauli  $Y$ -errors on the emitter spin between single-photon emissions. These errors are likely to be the dominant error mechanism in quantum dot implementations of the proposal. Both the direct and the  $\langle ZXZ \rangle$  bound can provide two different figures of merit for such a source. First, the number of qubits across which the LE is non-zero can be considered; second, the value of the LE across a fixed number of qubits constitutes a figure of interest. As shown in Fig. 4, the  $\langle ZXZ \rangle$  bound is considerably below the direct bound for both quantities. The  $\langle ZXZ \rangle$  bound approaches the direct bound as  $\langle ZXZ \rangle \rightarrow 1$  (see the inset in Fig. 4).

The  $\langle ZXZ \rangle$  bound is therefore particularly useful for sources with low emission/detection efficiencies and little decoherence of the emitter spin. In that case, no direct bound is available but  $\langle ZXZ \rangle$  is close to unity and hence high values of LE across a fixed number of qubits as well as non-zero LE across many qubits can be demonstrated.

## VI. CONCLUSION

Our result for the worst-case localizable entanglement in a cluster state approximation provides a benchmark for sources of large photonic cluster states that could enable experimental MBQC protocols in the future. We have shown that as the measured three-photon correlation  $\langle ZXZ \rangle$  approaches unity, useful entanglement increases at a rate lower-bounded by Eq. (11). The method of lower bounding stabilizer expectation values by expectation values of the stabilizer generators possibly has applications in the investigation of other stabilizer states.

The measurement of  $\langle ZXZ \rangle$  can be accomplished with the simple setup shown in (2) and emission/detection efficiencies that are already available. The threshold for establishing a cluster state source capable of producing long-range entanglement is therefore lowered to demonstrating  $\langle ZXZ \rangle > \frac{2}{3}$ , which would demonstrate non-zero localizable entanglement across a single qubit. The experiment reported in Ref. 10 comes close to this threshold.

We wish to acknowledge a related bound on the fidelity of a state with the ideal cluster state given  $\langle ZXZ \rangle$  that was presented in Ref. 19. Interestingly the state  $\rho^{\text{WC}}$  also saturates this fidelity bound which was obtained with seemingly different methods.

## ACKNOWLEDGMENTS

We gratefully acknowledge fruitful discussions with David Jennings and Ilai Schwarz and the support of the United States Army Research Office and the EPSRC.

## APPENDIX A: THREE EXPECTATION VALUES CAN LOWER BOUND THE LE

In Ref. 11, a bound on the LE was derived given three expectation values and assuming zero entanglement fluctuations<sup>14</sup> (“outcome-independent entanglement”). In the following, we show that this bound holds even in the presence of entanglement fluctuations. We only deal with qubits and projective measurements here.

**Theorem.** *The expectation values of three multi-qubit Pauli operators  $B_1$ ,  $B_2$ , and  $B_3$  lower bound the LE as measured by a convex entanglement measure  $E$  between two target qubits  $t_1$ ,  $t_2$  in any state  $\rho$  of  $n$  qubits as*

$$\text{LE}^{t_1, t_2}(\rho) \geq E(\rho_B). \quad (\text{A1})$$

Here  $\rho_B = \frac{1}{4}(\mathbb{1} \otimes \mathbb{1} + \langle B_1 \rangle Z \otimes Y + \langle B_2 \rangle Y \otimes Z + \langle B_3 \rangle X \otimes X)$  and  $\{B_i\}$  need to satisfy the following:

- There exists a collection of  $n - 2$  single-qubit Pauli operators  $\{P_k\}$ , each acting on one of the  $n$  qubits except the target qubits  $t_1$ ,  $t_2$ , such that  $[B_l, P_k] = 0 \forall l, k$ . The label  $k$  runs from 0 to  $n - 2$ , while the target qubits are labelled  $t_1, t_2$ .
- $B_3 = B_2 B_1$ .
- All three operators  $B_i$  have nontrivial support on both qubits  $t_1$  and  $t_2$ , i.e., the component of  $B_i$  acting on the  $t_1, t_2$  subspace is some two-qubit Pauli operator  $B_i^t$ .

*Proof.* The LE between qubits  $t_1$  and  $t_2$  in an  $n$ -qubit state  $\rho$  is defined as<sup>14</sup>

$$\text{LE}^{t_1, t_2}(\rho) := \sup_{\{m\}} \sum_s p_s E(\rho_{m, s}^{t_1, t_2}). \quad (\text{A2})$$

Here  $\{m\}$  denotes all possible sequences of local measurements on the  $n - 2$  qubits other than  $t_1$ ,  $t_2$ , binary string  $s$  gives the outcomes of such a measurement sequence, and  $p_s$  is the probability of this outcome.  $\rho_{m, s}^{t_1, t_2}$  is the state of qubits  $t_1$ ,  $t_2$  after a particular measurement sequence  $m$  with outcomes  $s$ .

The state of qubits  $t_1$ ,  $t_2$  obtained from  $\rho$  by the measurement sequence  $\{P_k\}$  with outcomes  $s$  is written  $\rho_{\{P_k\}, s}^{t_1, t_2}$ . The average entanglement obtained by  $\{P_k\}$  is

$$\sum_s p_s E(\rho_{\{P_k\}, s}^{t_1, t_2}), \quad (\text{A3})$$

and clearly lower bounds  $\text{LE}^{t_1, t_2}(\rho)$ . Furthermore

$$E(\rho_{\{P_k\}, s}^{i, j}) \geq E(\rho_s), \quad (\text{A4})$$

where  $\rho_s := \frac{1}{4}(\mathbb{1} + t_1 B_1^t + t_2 B_2^t + t_3 B_3^t)$  (additional terms cannot decrease entanglement<sup>11</sup>). The coefficients  $t_i$  are the expectation values of the corresponding two-qubit Pauli operators  $B_i$  in the state  $\rho_{\{P_k\}, s}^{t_1, t_2}$ .

We now associate strings of  $n - 2$  bits with operators  $Q_q$  on the  $n - 2$  qubits other than  $t_1, t_2$  where 1 (0) at position  $k$  in  $q$  means that the component of  $Q_q$  acting on qubit  $k$  is  $P_k$  ( $\mathbb{1}_k$ ). For instance, we have  $Q_{01101} = \mathbb{1}_1 \otimes P_2 \otimes P_3 \otimes \mathbb{1}_4 \otimes P_5$ .

With this notation, the coefficients  $t_i$  in  $\rho_s$  are related to expectation values in the  $n$  qubit state  $\rho$  (write  $\langle \hat{O} \rangle = \text{Tr}[\hat{O}\rho]$ ) as

$$t_i = \sum_q \frac{(-1)^{s \cdot q}}{2^{n-2} p_s} \langle B_i^t \otimes Q_q \rangle. \quad (\text{A5})$$

The sum runs over all  $2^{n-2}$  bit strings  $q$  of length  $n-2$ .  $s \cdot q$  denotes the modular sum of all those measurement outcomes  $s_i$  where  $q_i = 1$ . One of the terms in the sum of (A5) corresponds to the known expectation value  $\langle B_i \rangle = \langle B_i^t \otimes Q_{q_{B_i}} \rangle$ .

We can now exploit the convexity of our entanglement measure  $E$  and invariance of entanglement under local unitary operations  $U_s$  to write

$$\begin{aligned} \text{LE}^{t_1, t_2}(\rho) &\geq \sum_s p_s E(\rho_s) = \sum_s p_s E(U_s \rho_s U_s^\dagger) \\ &\geq E\left(\sum_s p_s U_s \rho_s U_s^\dagger\right). \end{aligned} \quad (\text{A6})$$

The local unitary  $U_s$  can be chosen as a tensor product of two Pauli operators such that it anticommutes with two of the three  $B_i^t$ . For example, if  $B_1^t = Z \otimes Y$ ,  $B_2^t = Y \otimes Z$ , and  $B_3^t = X \otimes X$ , we could choose  $U_s = Z \otimes \mathbb{1}$  for a particular  $s$  and have  $U_s B_1 U_s^\dagger = B_1$ ,  $U_s B_2 U_s^\dagger = -B_2$ , and  $U_s B_3 U_s^\dagger = -B_3$ . We then associate with every choice of  $U_s$  a triplet of binary numbers  $f_{1,2,3}(s)$  such that  $f_i(s) = 1$  if  $\{U_s, B_i^t\} = 0$  and  $f_i(s) = 0$  if  $[U_s, B_i^t] = 0$ . Note that  $f_1(s)$  and  $f_2(s)$  can be chosen freely, while  $f_3(s) = f_1(s) \oplus f_2(s)$ . The particular choice of  $\{U_s\}$  and associated  $f_i(s)$  made here is

$$f_i(s) = q_{B_i} \cdot s, \quad (\text{A7})$$

where  $q_{B_i}$  is the binary string giving the sequence of  $\mathbb{1}$  and  $P_k$  operators in  $B_i$ .

Finally the expectation value of  $B_i^t$  for the state  $\rho_{\text{mix}} := \sum_s p_s U_s \rho_s U_s^\dagger$  can be written using (A5) as

$$\text{Tr}[B_i^t \rho_{\text{mix}}] = \sum_s p_s \sum_q \frac{(-1)^{q \cdot s \oplus f_i(s)}}{2^{n-2} p_s} \langle B_i^t \otimes Q_q \rangle. \quad (\text{A8})$$

Substituting (A7) for  $f_i(s)$ , we find

$$\sum_s (-1)^{(q \oplus q_{B_i}) \cdot s} = \begin{cases} 2^{n-2}, & \text{when } q = q_{B_i}, \\ 0, & \text{otherwise.} \end{cases} \quad (\text{A9})$$

Hence the functions  $f(s, 1)$  and  $f(s, 2)$  can be chosen such that  $\rho_{\text{mix}} = \frac{1}{4}(\mathbb{1} \otimes \mathbb{1} + \langle B_1 \rangle B_1 + \langle B_2 \rangle B_2 + \langle B_3 \rangle B_3)$ . Without loss of generality, any triplet of two-qubit Pauli operators satisfying the properties required in the theorem can be chosen as  $B_1 = Z \otimes Y$ ,  $B_2 = Y \otimes Z$ , and  $B_3 = X \otimes X$  such that

$$\text{LE}^{t_1, t_2}(\rho) \geq E(\rho_B). \quad (\text{A10})$$

□

## APPENDIX B : IS THE $\langle \text{XZX} \rangle$ BOUND TIGHT?

We provide three items of evidence in support of our conjecture

$$\begin{aligned} \text{LE}^{1,n}(\rho_n^{\text{WC}}(\lambda)) &= \max\{0, 1 - n(1 - \langle \text{XZX} \rangle)\} \\ &= \max\{0, 2\lambda - 1\}. \end{aligned} \quad (\text{B1})$$

First, we show that all equatorial measurement sequences yield entanglement no higher than the  $\langle \text{XZX} \rangle$  bound; second, we show analytically that the claim holds for  $\rho_4^{\text{WC}}$ ; and finally, we present numerics for  $\rho_7^{\text{WC}}$ .

### 1. Equatorial measurement sequences

*Lemma.* Given  $\rho_n^{\text{WC}}(\lambda)$ , no sequence of equatorial measurements can produce a two-qubit state  $\rho_{1,n}$  with  $E(\rho_{1,n}) > 2\lambda - 1$ .

*Proof.* We first derive a form for the two-qubit state  $|\phi_{1,n}\rangle$  resulting from a sequence of equatorial measurements  $\mathcal{M}_e$  on qubits 2 to  $n-1$  in the  $n$ -qubit cluster state  $|C_n\rangle$ . An equatorial measurement projects onto either of the states  $|\varphi, s=0, 1\rangle = \frac{1}{\sqrt{2}}(|0\rangle + (-1)^s e^{i\varphi}|1\rangle)$ . Using the expression,

$$\begin{aligned} & (|\varphi, s\rangle\langle\varphi, s|_A \otimes \mathbb{1}_B) S_{AB}(|\Psi\rangle_A \otimes |+\rangle_B) \\ &= |\varphi, s\rangle_A \otimes X^s H(\varphi)|\Psi\rangle_B, \end{aligned} \quad (\text{B2})$$

where  $S_{AB}$  is the controlled phase gate and

$$H(\varphi) = \begin{pmatrix} 1 & e^{i\varphi} \\ 1 & -e^{i\varphi} \end{pmatrix}, \quad (\text{B3})$$

we find that

$$|\phi_{1,n}\rangle = \mathcal{N} \langle \vec{\varphi}, \vec{s} | C_n \rangle = (\mathbb{1}_1 \otimes U_n) |\phi^+\rangle_{1,n}. \quad (\text{B4})$$

Here  $|\phi^+\rangle$  denotes a maximally entangled state,  $\mathcal{N}$  is the normalization factor,

$$|\vec{\varphi}, \vec{s}\rangle = |\varphi_2, s_2\rangle_2 |\varphi_3, s_3\rangle_3 \cdots |\varphi_{n-1}, s_{n-1}\rangle_{n-1}, \quad (\text{B5})$$

and

$$U_n = X^{s_{n-1}} H(\varphi_{n-1}) \cdots X^{s_3} H(\varphi_3) X^{s_2} H(\varphi_2). \quad (\text{B6})$$

Without loss of generality, we can take  $s_i = 0$  when writing  $U_n$  in the following.

Furthermore we find that

$$\begin{aligned} \langle \vec{\varphi}, \vec{s} | Z_1 | C_n \rangle &\propto (\mathbb{1}_1 \otimes U_n X) |\phi^+\rangle_{1,n} \equiv |\phi_{1,n}^{Z_1}\rangle, \\ \langle \vec{\varphi}, \vec{s} | Z_j | C_n \rangle &\propto (\mathbb{1}_1 \otimes U_n^j) |\phi^+\rangle_{1,n} \equiv |\phi_{1,n}^{Z_j}\rangle, \\ \langle \vec{\varphi}, \vec{s} | Z_n | C_n \rangle &\propto (\mathbb{1}_1 \otimes (ZU)_n) |\phi^+\rangle_{1,n} \equiv |\phi_{1,n}^{Z_n}\rangle, \end{aligned} \quad (\text{B7})$$

where  $U_n^j$  is given by  $U_n$  from (B6) with  $s_j = 1$  and  $s_i = 0 \forall i \neq j$ . The state  $\rho_{1,n}$  resulting from  $\mathcal{M}_e$  on  $\rho_n^{WC}$  is therefore given by

$$\begin{aligned} \rho_{1,n} &= \mathcal{N} \langle \vec{\varphi}, \vec{s} | \rho_n^{WC} | \vec{\varphi}, \vec{s} \rangle \\ &= \lambda |\phi_{1,n}\rangle\langle\phi_{1,n}| + \frac{1-\lambda}{n} |\phi_{1,n}^{Z_1}\rangle\langle\phi_{1,n}^{Z_1}| \\ &\quad + \frac{1-\lambda}{n} \sum_{j=2}^{n-1} |\phi_{1,n}^{Z_j}\rangle\langle\phi_{1,n}^{Z_j}| + \frac{1-\lambda}{n} |\phi_{1,n}^{Z_n}\rangle\langle\phi_{1,n}^{Z_n}|. \end{aligned}$$

We now observe that for  $1 \leq i \leq n$ ,

$$C(\lambda |\phi_{1,n}\rangle\langle\phi_{1,n}| + (1-\lambda) |\phi_{1,n}^{Z_i}\rangle\langle\phi_{1,n}^{Z_i}|) = 2\lambda - 1, \quad (\text{B8})$$

as  $|\phi_{1,n}\rangle\langle\phi_{1,n}|$  and  $|\phi_{1,n}^{Z_i}\rangle\langle\phi_{1,n}^{Z_i}|$  are orthogonal, maximally entangled states. Therefore, by convexity of concurrence,

$$E(\rho_{1,n}) \leq 2\lambda - 1. \quad (\text{B9})$$

□

## 2. Analytics for $\rho_4^{WC}$

We derive an exact expression for the concurrence of the two-qubit state resulting from two measurements in the  $X$ - $Z$  plane on the middle qubits in the four-qubit WC state. The result substantiates our conjecture that general measurement sequences on  $\rho_n^{WC}$  cannot reach higher entanglement than equatorial ones.

The result of a projective measurement on qubit  $i$  in the  $X$ - $Z$  plane may be written as  $|\theta_i\rangle = \cos \frac{\theta_i}{2} |0\rangle + \sin \frac{\theta_i}{2} |1\rangle$ . We perform measurements on qubits two and three of  $\rho_4^W$ , with outcomes parametrized by  $\theta_2$  and  $\theta_3$ , respectively. This yields the two-qubit state

$$\rho_{1,4} = \frac{1}{4} (\mathbb{1} \otimes \mathbb{1} + \vec{r} \cdot \vec{\sigma} \otimes \mathbb{1} + \mathbb{1} \otimes \vec{s} \cdot \vec{\sigma} + \sum_{i,j=1}^3 T_{ij} \sigma_i \otimes \sigma_j),$$

which has components

$$\vec{r} = \frac{1+\lambda}{2} \begin{pmatrix} \cos \theta_2 \\ 0 \\ \sin \theta_2 \cos \theta_3 \end{pmatrix}, \quad \vec{s} = \frac{1+\lambda}{2} \begin{pmatrix} \cos \theta_3 \\ 0 \\ \sin \theta_3 \cos \theta_2 \end{pmatrix},$$

$$T = \begin{pmatrix} \lambda \cos \theta_2 \cos \theta_3 & 0 & \lambda \sin \theta_3 \\ 0 & (2\lambda - 1) \sin \theta_2 \sin \theta_3 & 0 \\ \lambda \sin \theta_2 & 0 & 0 \end{pmatrix}.$$

The entanglement of a state is invariant under local unitary operations,  $\rho_{1,4} \rightarrow (U_1 \otimes U_4)\rho_{1,4}(U_1^\dagger \otimes U_4^\dagger)$ . This corresponds to the transformations  $\vec{r} \rightarrow O_1\vec{r}$ ,  $\vec{s} \rightarrow O_4\vec{s}$ , and  $T \rightarrow O_1 T O_4^T$ , where  $O_1$  and  $O_4$  are the orthogonal matrices.<sup>20</sup> By choosing  $O_1$  and  $O_4$  that achieve a signed singular value decomposition of  $T$ , we perform local unitary operations on  $\rho_{1,4}$  that correspond to the transformation

$$\rho_{1,4} \rightarrow \frac{1}{4} \begin{pmatrix} N_+(1+\lambda) & 0 & 0 & S(1-3\lambda) \\ 0 & 1-\lambda & S(\lambda-1) & 0 \\ 0 & S(\lambda-1) & 1-\lambda & 0 \\ S(1-3\lambda) & 0 & 0 & N_-(1+\lambda) \end{pmatrix},$$

where  $S = \sin \theta_2 \sin \theta_3$  and  $N_\pm = 1 \pm \sqrt{1 - S^2}$ .

The above density matrix is manifested in the form of an  $X$ -state.<sup>21</sup> The concurrence of such a state is a simple function of the density matrix elements, which for us gives

$$C(\rho_{1,4}) = \max\left\{0, \frac{1}{2}(3\lambda - 1)S + \frac{1}{2}(\lambda - 1)\right\}. \quad (\text{B10})$$

The entanglement that is localized by measurements in the  $X$ - $Z$  plane on  $\rho_4^W$  is therefore clearly maximized by the equatorial measurement sequence, which gives  $\sin \theta_2 = \sin \theta_3 = 1$  and hence  $S = 1$ .

### 3. Numerics for $\rho_7^{WC}$

We have not found an analytic form for  $\text{LE}^{1,n}(\rho_n^{WC})$  when  $n > 4$ . To further investigate whether our conjecture  $\text{LE}^{1,n}(\rho_n^{WC}) = 2\lambda - 1$  holds, we therefore perform a numerical optimization.

Using a Nelder-Mead simplex algorithm, the following optimization was carried out:

$$\max_{\vec{\theta}, \vec{\varphi}} C(\mathcal{N}\langle \vec{\theta}, \vec{\varphi} | \rho_7^W | \vec{\theta}, \vec{\varphi} \rangle), \quad (\text{B11})$$

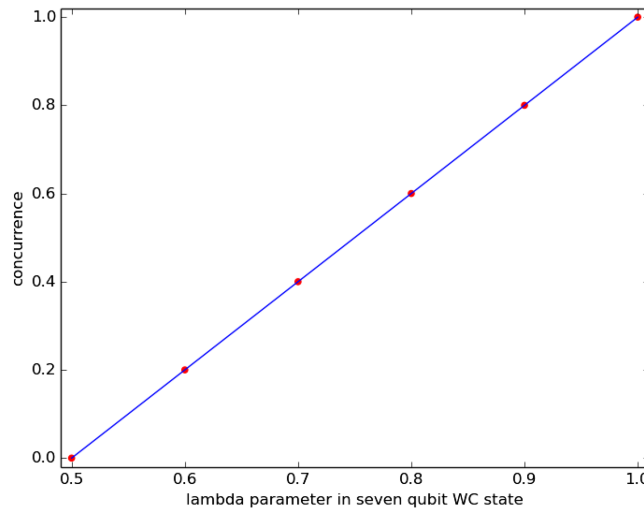


FIG. 5. Numerical optimization of the concurrence of the two-qubit state resulting from five single-qubit measurements on  $\rho_7^W$ . The red dots show the maximum entanglement obtained while the blue line gives the value  $2\lambda - 1$  of the  $\langle ZXZ \rangle$  bound.

where  $\mathcal{N}$  gives the normalization factor and

$$|\vec{\theta}, \vec{\varphi}\rangle = \otimes_{i=2}^6 \left( \sin \frac{\theta_i}{2} |0\rangle_i + e^{i\varphi_i} \cos \frac{\theta_i}{2} |1\rangle_i \right). \quad (\text{B12})$$

The results for six different values of  $\lambda$  are shown in Fig. 5. We find that the optimal measurement angles are  $\theta_i = \frac{\pi}{2}$  and that  $\varphi_i$  is arbitrary. This yields a value of concurrence  $C(\rho_{1,7}) = 2\lambda - 1$ , again providing evidence for the conjecture  $\text{LE}^{1,n}(\rho_n^{WC}) = 2\lambda - 1$ .

- <sup>1</sup> R. Raussendorf, D. E. Browne, and H. J. Briegel, *Phys. Rev. A* **68**, 022312 (2003).
- <sup>2</sup> D. Gross, J. Eisert, N. Schuch, and D. Perez-Garcia, *Phys. Rev. A* **76**, 052315 (2007).
- <sup>3</sup> H. J. Briegel and R. Raussendorf, *Phys. Rev. Lett.* **86**, 910 (2001).
- <sup>4</sup> T.-C. Wei, I. Affleck, and R. Raussendorf, *Phys. Rev. A* **86**, 032328 (2012).
- <sup>5</sup> M. A. Nielsen, *Phys. Rev. Lett.* **93**, 040503 (2004).
- <sup>6</sup> D. E. Browne and T. Rudolph, *Phys. Rev. Lett.* **95**, 010501 (2005).
- <sup>7</sup> M. Gimeno-Segovia, P. Shadbolt, D. E. Browne, and T. Rudolph, *Phys. Rev. Lett.* **115**, 020502 (2015).
- <sup>8</sup> N. H. Lindner and T. Rudolph, *Phys. Rev. Lett.* **103**, 113602 (2009).
- <sup>9</sup> S. E. Economou, N. Lindner, and T. Rudolph, *Phys. Rev. Lett.* **105**, 093601 (2010).
- <sup>10</sup> I. Schwartz, D. Cogan, E. R. Schmidgall, Y. Don, L. Gantz, O. Kenneth, N. H. Lindner, and D. Gershoni, *Science* **354**, 434 (2016).
- <sup>11</sup> I. Schwarz and T. Rudolph, *Phys. Rev. A* **85**, 050306 (2012).
- <sup>12</sup> D. D. B. Rao, S. Yang, and J. Wrachtrup, *Phys. Rev. B* **92**, 081301 (2015).
- <sup>13</sup> M. Bayer, G. Ortner, O. Stern, A. Kuther, A. A. Gorbunov, A. Forchel, P. Hawrylak, S. Fafard, K. Hinzer, T. L. Reinecke, S. N. Walck, J. P. Reithmaier, F. Klopff, and F. Schäfer, *Phys. Rev. B* **65**, 195315 (2002).
- <sup>14</sup> M. Popp, F. Verstraete, M. A. Martn-Delgado, and J. I. Cirac, *Phys. Rev. A* **71**, 042306 (2005).
- <sup>15</sup> M. A. Nielsen and I. L. Chuang, *Quantum Computation and Quantum Information*, 10th ed. (Cambridge University Press, Cambridge, New York, 2010).
- <sup>16</sup> F. Verstraete, J. Dehaene, and B. DeMoor, *Phys. Rev. A* **64**, 010101 (2001).
- <sup>17</sup> J. Grondalski, D. M. Etlinger, and D. F. V. James, *Phys. Lett. A* **300**, 573 (2002).
- <sup>18</sup> M. Horodecki, P. Horodecki, and R. Horodecki, *Phys. Rev. A* **60**, 1888 (1999).
- <sup>19</sup> M. Cramer, M. B. Plenio, S. T. Flammia, R. Somma, D. Gross, S. D. Bartlett, O. Landon-Cardinal, D. Poulin, and Y.-K. Liu, *Nat. Commun.* **1**, 149 (2010).
- <sup>20</sup> R. Horodecki and M. Horodecki, *Phys. Rev. A* **54**, 1838 (1996).
- <sup>21</sup> T. Yu and J. H. Eberly, *Quantum Inf. Comput.* **7**, 459 (2007), see <http://www.rintonpress.com/xqic7/qic-7-56/459-468.pdf>.